Citation for final published version:

Shen, Zhengtao, Zhang, Yunhui, Jin, Fei , Alessi, Daniel, Zhang, Yiyun, Wang, Fei, McMillan, Oliver and Al-Tabbaa, Abir 2018. Comparison of nickel adsorption on biochars produced from mixed softwood and Miscanthus straw. Environmental Science and Pollution Research 25 , 14626–14635. 10.1007/s11356-018-1674-2

Publishers page: https://link.springer.com/article/10.1007/s11356-0...

Comparison of nickel adsorption on biochars produced from mixed softwood and *miscanthus* straw

Zhengtao Shen [a, b, 1, *], Yunhui Zhang [a, 1], Fei Jin [c], Daniel S. Alessi [b], Yiyun Zhang [a], Fei Wang [a, d, *], Oliver McMillan [a], Abir Al-Tabbaa [a]

[a] Geotechnical and Environmental Research Group, Department of Engineering, University of Cambridge, Cambridge CB2 1PZ, United Kingdom

[b] Department of Earth and Atmospheric Sciences, University of Alberta, Edmonton T6G 2E3, Canada

[c] School of Engineering, University of Glasgow, Glasgow G12 8QQ, UK

[d] Institute of Geotechnical Engineering, School of Transportation, Southeast University, Nanjing 210096, China

* Corresponding author:

Zhengtao Shen, Email: ztshennju@gmail.com; zshen4@ualberta.ca

& Fei Wang, Email: 101012020@seu.edu.cn

[1] These authors contributed equally to this work

Abstract: In order to understand the influence of feedstock type on biochar adsorption of heavy metals, the adsorption characteristics of nickel (Ni^{2+}), copper (Cu^{2+}) and lead (Pb^{2+}) onto biochars derived from mixed softwood and *miscanthus* straw were compared. The biochars were produced from mixed softwood pellets (SWP) and *miscanthus* straw pellets (MSP), at both 550 °C and 700 °C for each material, using a standardised production procedure recommended by the UK Biochar Research Centre. Kinetics analyses show that the adsorption of Ni^{2+} to all four biochars reached equilibrium within 5 minutes. The degree of Ni^{2+} removal for all four biochars remained nearly constant within initial pH values of 3-8, because the equilibrium pH values within this range were similar due to the buffering effect of the biochars. A sharp increase of Ni^{2+} removal percentage for all biochars at initial solution pH 8-10 was observed as the equilibrium pH also increased. MSP derived biochars generally had higher maximum adsorption capacities (Q_{max}) for the three tested metals as compared with those from SWP, which was likely due to their higher degree of carbonisation during production. This study shows that feedstock type is a primary factor affecting the adsorption capacities of the tested biochars for heavy metals.

Keywords: biochar, remediation, adsorption, heavy metal, softwood, *miscanthus* straw

1 Introduction

Environmental pollution in air, land, and water has been a huge challenge to the modern society (Hou and Li 2017; Qi et al. 2017; P. Zhang et al. 2017). The sustainable remediation of contaminated environmental media has drawn great attention during recent years (Hou and Al-Tabbaa 2014; Hou et al. 2017a; Hou et al. 2017b; Song et al. 2018). Biochar is regarded as an emerging and sustainable sorbent for heavy metal remediation of water and soil, due to its multiple additional environmental benefits including waste management, energy production, carbon storage and soil improvement (Ronsse et al. 2013; Lehmann 2007; Cao et al. 2011; Beesley et al. 2011; Shen et al. 2016; Shen et al. 2017a). Key to applying biochar for these purposes is an understanding of the adsorption characteristics of heavy metals, in order to aid in its practical application in water and soil remediation.

Biochar properties are highly dependent on the type of feedstock used (Zhang et al. 2017a). Plant, sewage sludge, manure and bones are raw materials often used for biochar production (Li et al. 2017), and plants obtained from agriculture wastes are among the most typical types of biomass used as biochar feedstock. Plants mainly consist of lignin, cellulose, hemicellulose and inorganic minerals, and the content of each component varies as a function of the plant type. Taking wood and wheat straw, two of the most frequently used feedstocks for biochar, as examples, wood contains more lignin (25-30% for wood versus 15-20% for wheat straw) and less inorganic minerals than does straw (Jahirul et al. 2012). The differing thermal decomposition patterns of each component during heating (Jahirul et al. 2012) results in biochars with significantly different properties and consequently differing metal adsorption behaviours. Heavy metal is an important class of environmental pollutants that may originate from various anthropogenic sources and are widely distributed (Hou et al. 2016, 2017c; Ma et al. 2015, 2014). A range of laboratory studies have revealed the adsorption characteristics of heavy metals on biochars produced from a particular plant biomass (*e.g.*, Park et al. 2015; Shen et al. 2015; Chi et al. 2017). However, the biochar production parameters, including highest heating temperature, heating rate, residence time, protection gas and quality control, vary widely among these studies. It is therefore difficult to isolate the influence of feedstock type on the adsorption of heavy metals by biochar. Although comparison of the adsorption of heavy metals among biochars, produced from different plant biomass under same conditions, has been conducted in several previous studies (Wang et al. 2016; Mohan et al. 2007), it has not been extensively investigated, especially for biochars produced under highly controlled pyrolysis conditions and having high reproducibility.

In order to aid the selection of the most suitable biochars for treatment of heavy metals in soil and water, it is critical to understand the influence of feedstock type on biochar adsorption of heavy metals after eliminating other influencing factors. To that end, in this study, mixed softwood and *miscanthus* straw biochars were obtained from the UK Biochar Research Centre (UKBRC), which aims to produce standardised biochars. A high degree of reproducibility of these standard biochars can be achieved because the production process and pyrolysis conditions are carefully monitored. This enables to isolate in the current study the influence of feedstock type on biochar adsorption of three tested metals: nickel (Ni^{2+}), copper (Cu^{2+}) and lead (Pb^{2+}), using laboratory batch adsorption experiments.

2 Materials and methods

2.1 Biochar

Two types of feedstock biomass were used to produce the biochar used in this study: (1) mixed softwood pellets (SWP) and, (2) *miscanthus* straw pellets (MSP). Biochars were produced by the United Kingdom Biochar Research Centre (UKBRC) from both SWP and MSP at both 550 °C and 700 °C, resulting in four biochars hereafter referred to as SWP550, SWP700, MSP550 and MSP700. The standardised production procedure can be found on the website of UKBRC (UKBRC 2016). Upon receipt, the biochars were dried in an oven at 60 °C for 48 h and sieved to < 0.15 mm particle sizes before experimentation. The cation exchange capacity (CEC) of each biochar was tested using a compulsive exchange method based on Gillman and Sumpter (1986). Other physicochemical properties were obtained from the UKBRC (2016). The surface morphology of the biochar was examined by a scanning electron microscopy (SEM) at 15 kV after coating the samples with gold. The infrared spectrum of each biochar before and after Ni^{2+} adsorption was obtained using a TENSOR II Fourier transform infrared spectroscopy (FT-IR) spectrometer (Bruker), by taking 16 scans from 2000 to 700 cm^{-1} with a resolution of 1 cm^{-1}.

According to tests conducted by the UKBRC, the biochars predominantly consist of carbon (75.41-90.21%) (Table 1). SWP derived biochars have considerably lower pH than do those produced from MSP (7.91-8.44 versus 9.72-9.77). All four biochars are alkaline, with pH_{pzc} (point of zero charge) values between 7.8-7.9 (pH_{pzc} values can be obtained from adsorption study results of Mohan et al. (2014)). SWP derived biochars contain very low ash content (1.25-1.89%), while the content in MSP biochars is much higher (11.55-12.15%). Likewise, SWP derived biochars have lower P contents than MSP (0.06-0.07% versus 0.19-0.76%). The CECs and surface areas of the biochars are relatively low as compared with existing literature (Cui et al. 2015;

Chotpantarat et al. 2011), except for SWP700 which has a relatively high surface area (162.30 m^2 g^{-1}) suggesting a porous structure.

Table 1 Physicochemical properties of the biochars

	SWP550	SWP700	MSP550	MSP700
C (%)	85.52	90.21	75.41	79.18
H (%)	2.77	1.83	2.42	1.26
O (by difference) (%)	10.36	6.02	9.24	6.99
N (%)	<0.10	<0.10	0.78	1.03
P (%)	0.06	0.07	0.19	0.76
VM (%)	14.20	6.66	11.62	7.71
H:C	0.39	0.24	0.38	0.19
O:C	0.09	0.05	0.09	0.07
Total ash (%)	1.25	1.89	12.15	11.55
pH	7.91	8.44	9.77	9.72
pH_{pzc}*	7.8	7.9	7.8	7.8
BET surface area (m^2/g)	26.40	162.30	33.60	37.20
CEC (cmol/kg) *	2.53	2.56	5.95	10.80
Ni (mg/kg)	3.30	74.07	30.40	4.95
Cu (mg/kg)	19.41	9.66	26.64	5.88
Pb (mg/kg)	bdl	bdl	bdl	bdl

(VM = volatile matter, pH_{PZC} = point of zero charge, BET = Brunauer–Emmett–Teller, CEC = cation exchange capacity, bdl = below detection limit, the standard deviations (SD) for CEC were within 0.10-0.23, the SD for other properties can be found on UKBRC (2016), note that all the values are obtained from the UKBRC datasheet, except for those denoted with *)

2.2 Adsorption studies

Ni^{2+}, Cu^{2+} and Pb^{2+} were used as model divalent cations, to investigate the sorption of heavy metals to these biochars. The kinetics and both the influence of adsorbent dosage and solution pH on Ni^{2+} uptake from solution for all four biochars were investigated. The equilibrium adsorption of Ni^{2+}, Cu^{2+} and Pb^{2+} onto each of the biochars was also investigated.

Batch adsorption experiments were carried out in 50 mL polyethylene tubes in a temperature-controlled laboratory (20 ± 1 °C). The detailed experimental procedure of the adsorption studies can be found in Shen et al. (2017b). Briefly, for kinetics studies, 0.1 g biochar was added to 20 mL solutions of 5 mM $Ni(NO_3)_2$ (pH 5) (containing 0.01 M $NaNO_3$) and shaken at 200 rpm for 5 min, 10 min, 20 min, 30 min, 1 h, 2 h, 3 h, 6 h, 12 h or 24 h. The effect of adsorbent dosage on the equilibrium adsorption of Ni^{2+} was investigated by adding a measured amount of biochar (0.1, 0.2, 0.3, 0.4, 0.5, 0.6, 0.7, 0.8, 0.9 or 1 g) to 20 mL of 5 mM $Ni(NO_3)_2$ (containing 0.01 M $NaNO_3$) set to pH 5, and shaking those mixtures at 200 rpm for 24 h. The effect of solution pH on Ni^{2+} adsorption was investigated by adding 0.1 g of biochar to solutions containing 20 mL of 5 mM $Ni(NO_3)_2$ (containing 0.01 M $NaNO_3$), and subsequently shaking at 200 rpm for 24 h. The initial pH of each solution (before biochar addition) was adjusted to 2, 3, 4, 5, 6, 7, 8, 9 or 10. Solutions of 0.01M, 0.1 M and 1 M HNO_3 and 0.01M, 0.1 M and 1M NaOH were used to adjust the initial pH of the solutions where required. The equilibrium pH and the removal of Ni^{2+} were recorded. In order to distinguish between precipitated $Ni(OH)_2$ and adsorbed Ni^{2+} as a function of equilibrium pH, the fractions of Ni^{2+} removed via precipitation were calculated using Visual MINTEQ 3.1.

In order to construct metal adsorption isotherms for each biochar, 0.1 g biochar was added to 20 mL solutions (pH = 5) containing either Ni^{2+}, Cu^{2+} or Pb^{2+}, at concentrations of 0.1, 0.2, 0.3, 0.5, 1, 2, 3 or 5 mM (containing 0.01 M $NaNO_3$). The resulting mixtures were shaken at 200 rpm for 24 h to reach equilibrium. The equilibrium data were fit using linearized Langmuir and Freundlich models to reveal the maximum adsorption capacities and adsorption mechanisms of the metals on the biochars, as suggested by (Foo and Hameed 2010). The details of the models and calculations are given in Table S1.

2.3 Statistical analysis

All experiments were conducted in duplicates, and the means and standard deviations were calculated from these data. Linear regression was used to evaluate the fitness of the prediction models to the experimental data in this study using Origin 8.5. The suitability of the model fitting was assessed using R^2 values.

3 Results and discussion

3.1 FT-IR spectra and SEM images of biochars

The FT-IR spectra of the biochars are shown in Fig. 5. The peaks at 1575 cm^{-1} for SWP550 and MSP550 are attributed to aromatic C=C stretching (Keiluweit et al. 2010), and the peaks at 875, 800 and 750 cm^{-1} for SWP550 and MSP550 are attributed to aromatic C-H bending (Keiluweit et al. 2010), indicating an aromatic structure of the two biochars. Less peaks associated with aromatic C were observed on SWP700 and MSP700, suggesting that more condensed aromatic structure with less functional groups was formed, as increased peak temperature. The big peak between 1030-1080 cm^{-1} for MSP550 is attributed to C-O-C stretching vibrations resulted from cellulose and hemicellulose (Keiluweit et al. 2010). With increased peak temperature, cellulose and hemicellulose in the *miscanthus* straw further decomposed, resulting in less C-O-C groups. Therefore, this big peak diminished on FT-IR spectra of MSP700. Wood typically contain less cellulose and hemicellulose and more lignin than straw (Jahirul et al. 2012), therefore, the C-O-C peak was not obvious for SWP derived biochars, or the cellulose and hemicellulose already decomposed due to less amount. The SEM images (Fig. 1) show the porous structures of the four biochars, which is typical for plant-derived biochars (Usman et al. 2016). The pore diameters are generally less than 5 um for all biochars. MSP derived biochars generally reveal smaller pores than WSP. The differences in the morphology due to production temperature were not obvious.

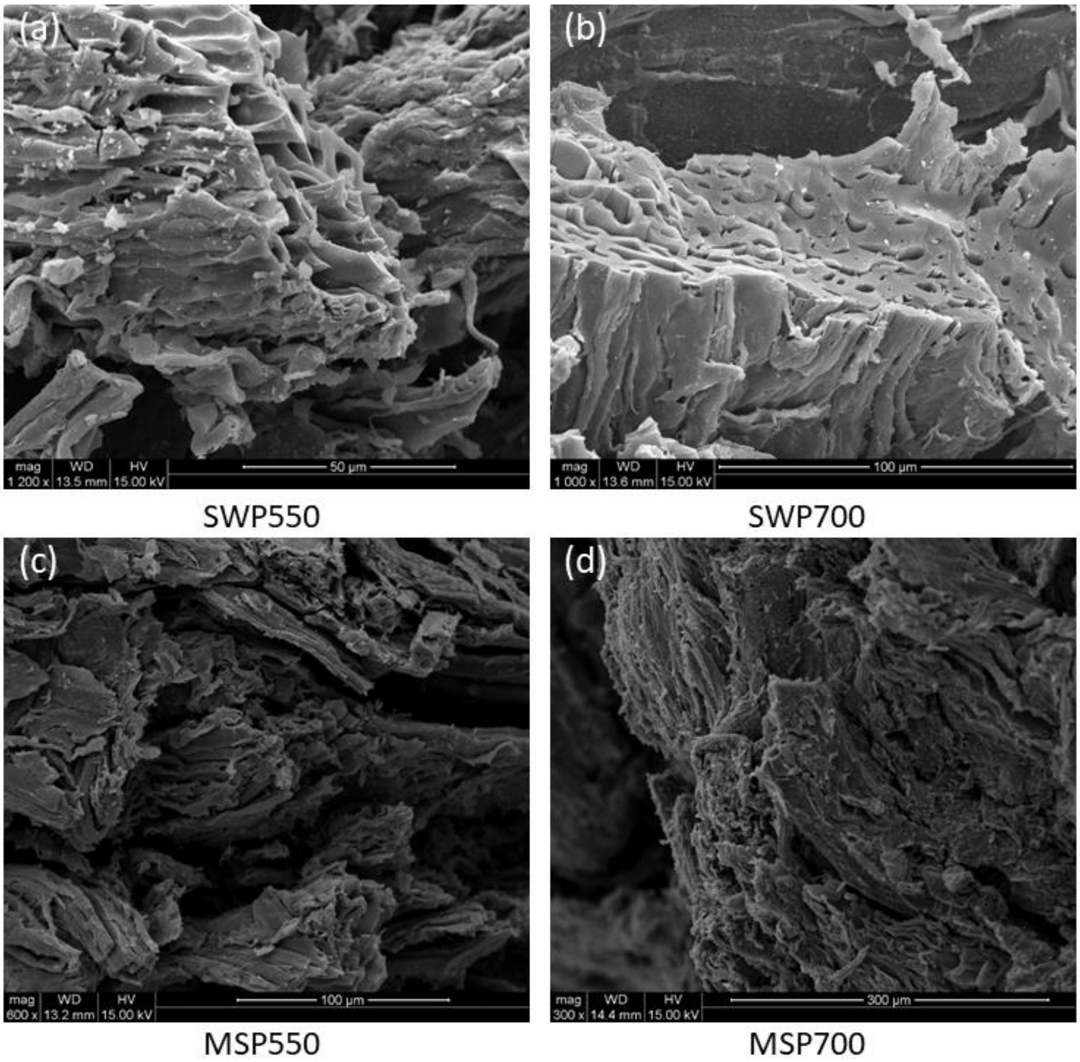

Fig. 1. SEM images of the biochars, including: (a) SWP550, (b) SWP700, (c) MSP550, and (d) MSP700.

3.2 Kinetics

The adsorption of Ni^{2+} to the four biochars reached equilibrium within 5 minutes (Fig. 2). Both the relatively high initial solution Ni^{2+} concentration (5 mM) and the fine biochar particle size (< 0.15 mm) likely contributed to this rapid adsorption. Higher adsorbate concentration in solution results in a larger chance for contact between the adsorbate and adsorbent surface, and therefore accelerated movement of adsorbate across the external liquid film boundary layer to external surface sites of the adsorbent (film diffusion) (Choy et al. 2004). Smaller particles have larger specific surface area, which may also aids the speed of film diffusion due to a larger solid – aqueous interface (Choy et al. 2004). In addition, the mass transport of adsorbate inside the adsorbent (intraparticle diffusion) becomes shorter as the radius of the adsorbent particle decreases, which also makes the adsorption faster (Choy et al. 2004; Rees et al. 2014). The rapid adsorption rate also suggests chemisorption (e.g. surface precipitation) may be a predominant mechanism for Ni^{2+} adsorption onto the four biochars, as chemisorption typically takes a shorter time, often within minutes (Inyang et al. 2015; Saleh et al. 2016; Tran et al. 2016).

The adsorption capacities (q_e) of Ni^{2+} on WSP550 and WSP700 were not significantly different, with both values between 0.03 and 0.05 mmol/g. In contrast, the q_e values for MSP derived biochars were significantly higher. The q_e for MSP700, around 0.35 mmol/g, was nearly double that of MSP550, suggesting that a higher production temperature aids in the adsorption capacity of MSP derived biochars.

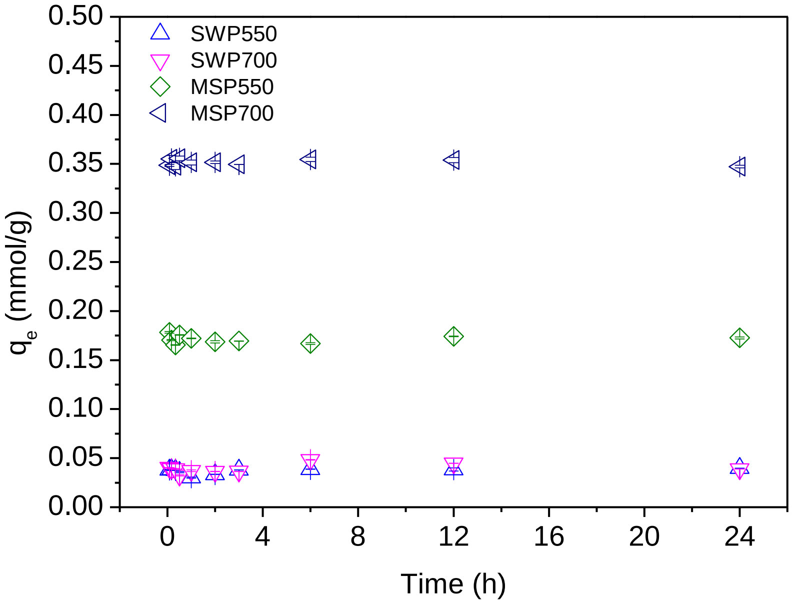

Fig. 2. Kinetics of Ni^{2+} adsorption on biochars (0.1 g biochar in 20 mL solution (0.01 M $NaNO_3$), initial Ni^{2+} concentration 5 mM; reaction temperature 20 °C; initial solution pH 5) (q_e - adsorption capacities).

3.3 Influence of adsorbent dosage

The influences of adsorbent dosage on Ni^{2+} removal and the adsorbed amount of Ni^{2+} per weight unit of biochar are shown in Fig. 3. The Ni^{2+} removal percentage for SWP550 increased from 3.97% to 16.63% across the adsorbent dosage range of 5-50 g/L. Likewise, the Ni^{2+} removal percentage for SWP700 increased from 3.89% to 20.54% at this range. Both biochars did not reach complete Ni^{2+} removal at the range of 5-50 g/L and exhibited low removal percentages compared with MSP derived biochars, suggesting a relatively low adsorption capacity of Ni^{2+} on SWP derived biochars. The adsorbed amount of Ni^{2+} per weight unit of biochar decreased in the range of 5-50 g/L for both of the SWP derived biochars.

In comparison to SWP derived biochars, the Ni^{2+} removal percentage for MSP550 increased from 17.28% to 98.03% as the adsorbent dosage increased from 5 to 40 g/L and remained at approximately 100% removal in the range of 40-50 g/L. The Ni^{2+} removal percentage for MSP700 increased from 18.29% to 99.67% at the adsorbent dosage range of 5-35 g/L and remained close to 100% removal up to 50 g/L. The adsorbed amount of Ni^{2+} per unit weight of biochar decreased as the adsorbent dosage increased from 5 to 50 g/L for both biochars. MSP-derived biochars generally show higher Ni^{2+} removal ability compared with SWP-derived biochars, which is in line with the kinetics findings.

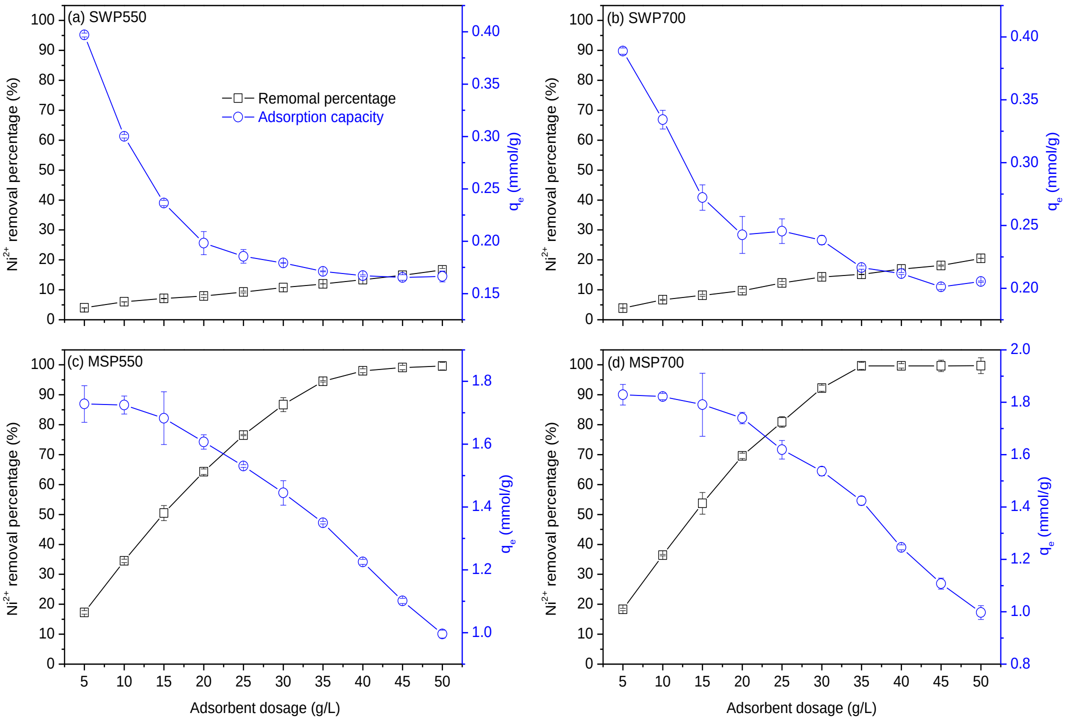

Fig. 3. The influence of adsorbent dosage on Ni^{2+} removal percentage and the adsorbed amount of Ni^{2+} per weight unit of biochar (mmol/g) (initial Ni^{2+} concentration 5mM in 20 mL solution (containing 0.01 M $NaNO_3$), reaction temperature 20 °C, initial solution pH 5, contact time 24 h).

3.4 Influence of solution pH

The influences of the initial solution pH on Ni^{2+} removal percentage and equilibrium solution pH values are shown in Fig. 4. The fraction of Ni^{2+} removed due to precipitation is also shown, which was calculated from the $Ni(OH)_2$ solubility data from the MINTEQ database. The high pH_{pzc} (7.8-7.9) suggests that the strong alkalinity of the biochars will aid in their adsorption for heavy metals through surface precipitation. It is of note that the pH near the biochar surface may be higher than the solution pH itself, and so even at lower solution pH, surface precipitation of metals may already have occurred. Therefore, there may be a discrepancy between the measured equilibrium solution pH and the conditions of precipitation calculated using MINTEQ.

The Ni^{2+} removal percentage for SWP derived biochars was low (3-5%) in the initial solution pH range of 2-7. It increased slightly to 9.82% at initial pH 8 before sharply increasing to 85.14% at initial pH 9 and subsequently increased to 99.50% at initial solution pH 10 for SWP550. For SWP700, it stayed within 3-5% at pH 8 and sharply increased to 85.82% at pH 9. It further increased to 99.79% at initial pH 10. The Ni^{2+} removal percentage for MSP550 increased from 3.41% to 15.44% as the initial solution pH increased from 2 to 4. It stayed nearly constant at the initial pH range of 4-8 before significantly increasing to 98.45% at initial pH 9, and remained at nearly complete removal at initial pH 10. The Ni^{2+} removal percentage for MSP700 increased from 1.56% to 18.14% with the increase of initial solution pH from 2 to 4. It was nearly constant within the initial pH range of 4-7 and slightly increased to 33.33% at pH 8. A sharp increase occurred between initial solution pH 8-9, nearing complete removal at initial pH 9-10. The changes in the precipitation of $Ni(OH)_2$ did not have a significant effect on Ni^{2+} removal between pH 2 and 9.

The Ni^{2+} removal percentages for SWP derived biochars were closely related to the equilibrium solution pH values. The Ni^{2+} removal percentages remained nearly constant within initial pH values of 3-8, because the equilibrium pH values at this range were relatively stable resulting from the buffing effect of the biochars. The insignificant increase of Ni^{2+} removal percentages at initial pH 2-4 for SWP derived biochars was likely due to proton competition with Ni^{2+} for adsorption onto biochar surface functional groups (Uchimiya et al. 2012). The sharp increase of Ni^{2+} removal percentage for all biochars at initial solution pH 8-10 likely occurred because the pH_{pzc} values of the biochars were exceeded. Under these conditions, the biochar surfaces became negatively charged, which enhanced adsorption of Ni^{2+} through electrostatic interactions. In addition, $Ni(OH)_2$ starts to precipitate on biochar surfaces at this range, which likely also contributed to the sharp increase of Ni^{2+} removal from solution.

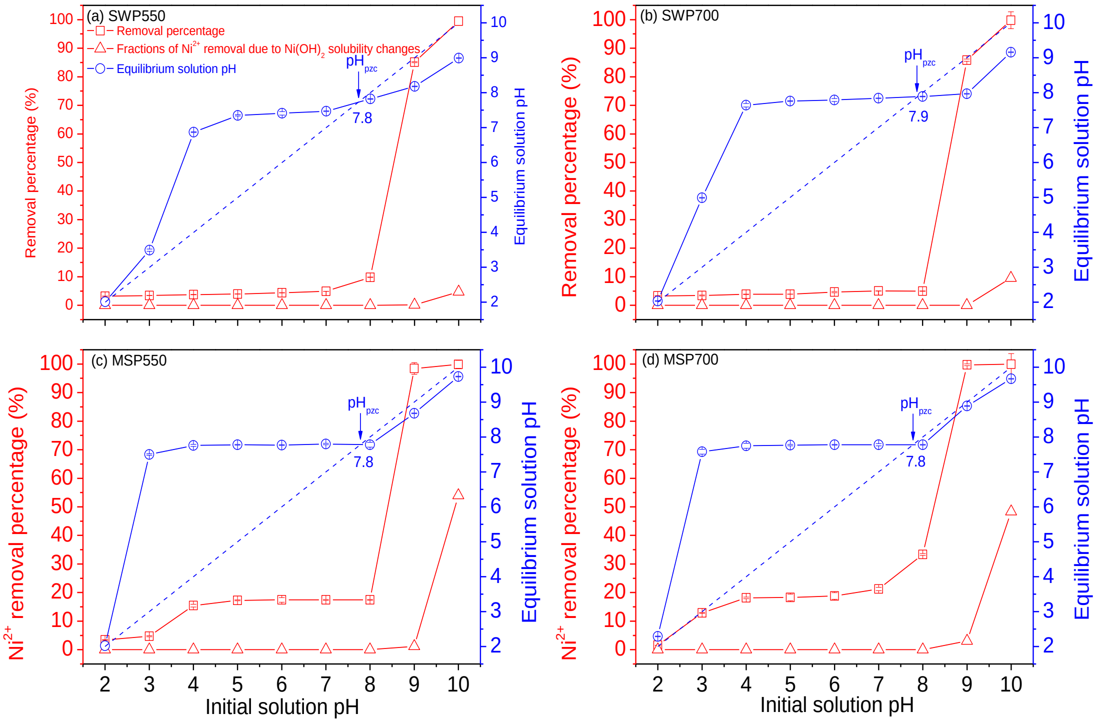

Fig. 4. The influence of initial solution pH on the Ni^{2+} removal percentage (red squares with solid lines), the equilibrium solution pH (blue circles with solid lines) and the fractions of Ni^{2+} removal due to the solubility change of $Ni(OH)_2$ (red triangles with solid lines); the dashed line is used to obtain the pH_{pzc} (initial Ni^{2+} concentration 5 mM, 0.1 g biochar in 20 mL solution (containing 0.01 M $NaNO_3$), reaction temperature 20 °C, contact time 24 h).

3.5 Adsorption equilibrium

Data from the equilibrium metal adsorption experiments conducted at room temperature for Ni^{2+} adsorption on biochars were modelled using isotherm approaches. Those for Cu^{2+} and Pb^{2+} were also obtained for comparison (Figs. S1, S2, S3 and Table 2). All isotherms are better fit by the Langmuir model than by the Freundlich model, except for Ni^{2+} adsorption on MSP550 and MSP700, indicating a monolayer adsorption of heavy metals on the biochars. Ni^{2+} adsorption on MSP550 and MSP700 reveals slightly higher R^2 values for the Freudlich model than for the Langmuir model, suggesting a certain degree of heterogeneity of the adsorption sites on MSP550 and MSP700 surfaces. The maximum adsorption capacity (Q_{max}) of heavy metals on biochars can be calculated using the Langmuir model, and MSP derived biochars reveal significantly higher Q_{max} values than do SWP for all three metals (Table 2). Pb^{2+} generally has higher Q_{max} values than do Ni^{2+} and Cu^{2+} on the MSP derived biochars, due to its lower hydration energy, which coincides with many previous findings (Shen et al. 2015; Liu et al. 2013). For SWP derived biochars, the Q_{max} values for the three metals vary considerably, and so there is not a specific metal that has the highest Q_{max} values.

Table 2 Parameters and regression coefficient of the equilibrium data for Ni^{2+}, Cu^{2+} and Pb^{2+} adsorption on the biochars fitted by the linear Langmuir and Freundlich isotherm models.

		Langmuir			Freundlich		
Metal	Biochar	Q_{max} (mmol/g)	b (L/mmol)	R^2	K_f	1/n	R^2
Ni^{2+}	SWP550	0.057	0.535	0.979	0.018	0.540	0.959

	SWP700	0.043	1.821	0.963	0.024	0.353	0.954
	MSP550	0.157	161.579	0.865	0.146	0.157	0.899
	MSP700	0.196	123.481	0.682	0.179	0.145	0.699
Cu^{2+}	SWP550	0.019	13.321	0.999	0.017	0.088	0.955
	SWP700	0.086	4.785	0.985	0.061	0.226	0.980
	MSP550	0.130	133.062	0.999	0.112	0.103	0.275
	MSP700	0.229	351.633	0.994	0.198	0.233	0.343
Pb^{2+}	SWP550	0.039	33.437	0.999	0.037	0.081	0.904
	SWP700	0.079	909.290	0.9999	0.074	0.079	0.375
	MSP550	0.183	-407.054	0.9998	0.164	0.151	0.467
	MSP700	0.357	23.907	0.998	0.318	0.315	0.451

3.6 Adsorption mechanisms and discussion

Biochar can adsorb heavy metals through a range of mechanisms including physical sorption, cation exchange, cation-π interaction, surface complexation and surface precipitation (Shen et al. 2017b). The FT-IR spectra (Fig. 5) generally show slight decrease of the peaks representing aromatic C=C and aromatic C-H of all four biochars after Ni^{2+} adsorption. This suggests that cation-π interaction, which is closely related to aromatic C (Keiluweit and Kleber 2009), may be a mechanism for Ni^{2+} adsorption on the four biochars. The peaks representing C-O-C stretching also decreased after Ni^{2+} adsorption for MSP derived biochars. This C-O-C belongs to acid derivatives (Keiluweit 2010), suggesting cation exchange or complexation, associated with acidic groups, may also contribute to Ni^{2+} adsorption on MSP derived biochars.

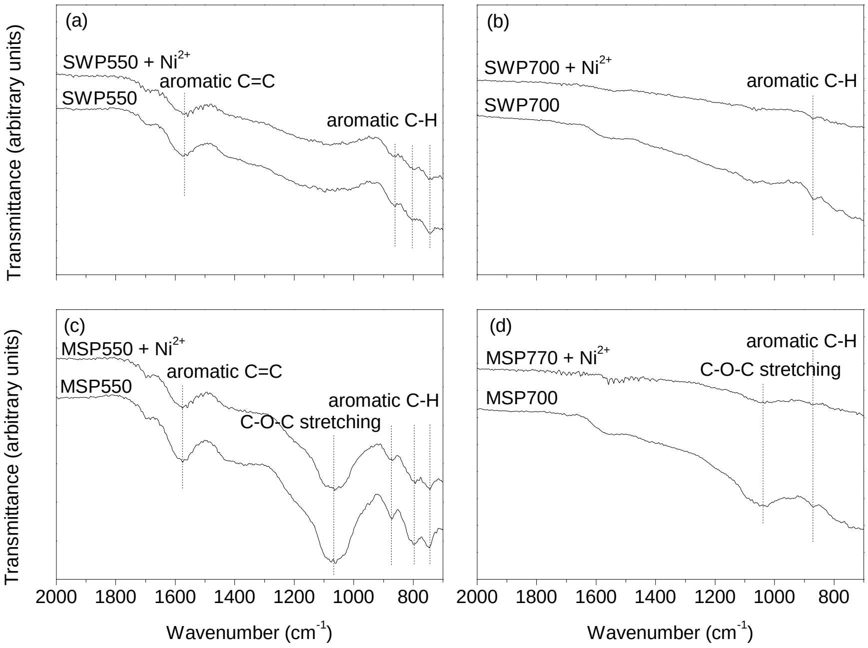

Fig. 5. FT-IR spectra of biochars before and after Ni^{2+} adsorption (the post Ni^{2+} adsorption sample was obtained from those for isotherm tests at 5 mM).

A previous study observed that surface precipitation and cation-π interaction are the main mechanisms contributing to heavy metal adsorption for biochars produced from other feedstocks (wheat straw and rice husk) but under the same production processes as those used in the present study (Shen et al. 2017b). In the present study, the high solution-pH dependence of the adsorption capacity of the four biochars for Ni^{2+} (Fig. 4) suggests that surface precipitation or cation-π interaction are the primary adsorption mechanisms, as they are both highly pH-dependent. As mentioned above, wood typically has higher lignin content than does *miscanthus*, but lower inorganic minerals. The incomplete carbonation of the feedstock during production of biochar, due to more ligneous material which is more thermally resistant, can result SWP derived biochars with less alkaline minerals (e.g., K_2O) (Dodson 2011), as is indicated by lower pH (Table 1) as well as in lower contents of inorganic compounds (e.g. CO_3^{2-} and PO_4^{3-}) for metal precipitation.

Therefore, SWP derived biochars may have adsorbed Ni^{2+} through surface precipitation and cation-π interaction. In comparison, MSP derived biochars may have stronger ability to precipitate Ni^{2+} compared with SWP. MSP derived biochars may also adsorb Ni^{2+} through cation exchange and surface complexation, in addition to precipitation and cation-π interaction. Therefore, SWP derived biochars have lower adsorption capacities for Ni^{2+} and other two metals as compared with MSP. This indicates that feedstock type is an important factor affecting the adsorption capacities of biochars for heavy metals.

For the same feedstock, a higher production temperature generally results in a higher adsorption capacity for the metals (Table 2). Higher production temperature promotes the carbonisation process of the feedstock and therefore aids the formation of more alkaline minerals, which will aid in the precipitation of metals to biochar surfaces. Although the pH and ash content were not significantly different between MSP550 and MSP700, the significantly lower O/C and H/C values for MSP700 suggests a higher degree of carbonisation and a higher aromaticity, which could provide MSP700 more aromatic π electrons for cation-π interactions with the metals (Keiluweit and Kleber 2009).

Apart from the adsorption capacity, the kinetics of metal uptake and the influence of solution pH on the degree of metal adsorption are similar for SWP and MSP derived biochars. Biochars produced from wheat straw and rice husk under the same standardised production process in a previous study (Shen et al. 2017c) also show similar trends in terms of kinetics and the influence of solution pH to Ni^{2+} adsorption. The faster kinetics of removal may be due to the small particle size of the biochars and the relatively high initial sorbate concentrations in solutions in both of the two studies.

4 Conclusions

This study investigates the adsorption characteristics of Ni^{2+}, Cu^{2+} and Pb^{2+} on

SWP and MSP derived biochars. The kinetics study shows that the adsorption of Ni^{2+} to all four biochars reached equilibrium rapidly (within 5 minutes), regardless of feedstock type and production temperature, which may be due to the small particle size of the biochars and relatively high initial sorbate concentrations in solutions. Likewise, the solution-pH dependence of Ni^{2+} adsorption for the four biochars shows a similar trend. There was an initial solution pH range of approximately 3-8, within which both the Ni^{2+} removal percentage and equilibrium solution pH remained nearly constant. This was due to a nearly constant equilibrium solution pH within the range, which resulted from the buffing effect of the biochars. Between the initial solution pH range of 8-10, the Ni^{2+} removal percentage dramatically increased to nearly 100%, corresponding to increased equilibrium solution pH. In general, the adsorption of Ni^{2+} on the four biochars was highly dependent on equilibrium solution pH. The biggest difference between the adsorption characteristics of SWP and MSP derived biochars are their adsorption capacities for all three metals. MSP derived biochars have significantly higher Q_{max} values than do those produced from SWP. Lignin and inorganic mineral contents may be the primary factors that cause the differences of adsorption capacity between SWP and MSP derived biochars.

Our study indicates that feedstock type is a primary factor affecting the adsorption capacities of biochar for heavy metals. As this study only includes adsorption studies, the influence of feedstock type on the desorption/reusability of the biochars are suggested for future work. More testing methods (e.g., X-ray absorption and X-ray diffraction) and surface complexation modelling may be used to aid in determining the mechanistic driving forces impacting the adsorption capacities of biochar for heavy metals in future studies.

Acknowledgements

The standard biochars were obtained from the UK Biochar Research Centre (UKBRC) at the University of Edinburgh. The authors would like to thank Dr. Ondrej Masek from the UKBRC for his kind help in preparing and delivering the biochar samples. Special thanks also go to Dr. Zhen Li from the College of Resources and Environmental Sciences, Nanjing Agricultural University, China, who conducted the SEM imaging for the biochars used in this study. The authors would also like to thank Tiesheng Wang and Rui Wu from the Department of Materials Science and Metallurgy at the University of Cambridge for conducting the FT-IR tests. The first author would like to thank the Killam Trusts from Canada for kindly providing the Izaak Walton Killam Memorial Postdoctoral Fellowship.

References

Beesley L, Moreno-Jiménez E, Gomez-Eyles JL, et al (2011) A review of biochars' potential role in the remediation, revegetation and restoration of contaminated soils. Environ Pollut 159:3269–82. doi: 10.1016/j.envpol.2011.07.023

Cao X, Ma L, Liang Y, et al (2011) Simultaneous immobilization of lead and atrazine in contaminated soils using dairy-manure biochar. Environ Sci Technol 45:4884–9. doi: 10.1021/es103752u

Chi T, Zuo J, Liu F (2017) Performance and mechanism for cadmium and lead adsorption from water and soil by corn straw biochar. Front Environ Sci Eng. doi: 10.1007/s11783-017-0921-y

Chotpantarat S, Ong SK, Sutthirat C, Osathaphan K (2011) Competitive sorption and transport of Pb2+, Ni2+, Mn2+, and Zn2+ in lateritic soil columns. J Hazard Mater 190:391–396. doi: 10.1016/j.jhazmat.2011.03.058

Choy KKH, Ko DCK, Cheung CW, et al (2004) Film and intraparticle mass transfer during the adsorption of metal ions onto bone char. J Colloid Interface Sci 271:284–295. doi: 10.1016/j.jcis.2003.12.015

Cui L, Yan J, Li L, et al (2015) Does Biochar Alter the Speciation of Cd and Pb in Aqueous Solution? BioResources. 10:88–104.

Dodson J (2011) Wheat straw ash and its use as a silica source. Ph.D. thesis dissertation. University of York.

Foo KY, Hameed BH (2010) Insights into the modeling of adsorption isotherm systems. Chem Eng J 156:2–10. doi: 10.1016/j.cej.2009.09.013

Gillman G, Sumpter E (1986) Modification to the compulsive exchange method for measuring exchange characteristics of soils. Aust J Soil Res 24:61. doi: 10.1071/SR9860061

Hou D, Al-Tabbaa A (2014) Sustainability: A new imperative in contaminated land remediation. Environ Sci Policy 39:25–34. doi: 10.1016/j.envsci.2014.02.003

Hou D, Ding Z, Li G, et al A Sustainability Assessment Framework for Agricultural Land Remediation in China.

Hou D, Gu Q, Ma F, O’Connell S (2016) Life cycle assessment comparison of thermal desorption and stabilization/solidification of mercury contaminated soil on agricultural land. J Clean Prod 139:949–956. doi: 10.1016/j.jclepro.2016.08.108

Hou D, Li F Complexities Surrounding China’s Soil Action Plan. L Degrad Dev.

Hou D, O’Connor D, Nathanail P, et al (2017a) Integrated GIS and multivariate statistical analysis for regional scale assessment of heavy metal soil contamination: A critical review.

Hou D, Qi S, Zhao B, et al (2017b) Incorporating life cycle assessment with health risk assessment to select the “greenest” cleanup level for Pb contaminated soil. J Clean Prod 162:1157–1168. doi: 10.1016/j.jclepro.2017.06.135

Inyang MI, Gao B, Yao Y, et al (2015) A Review of Biochar as a Low-Cost Adsorbent for Aqueous Heavy Metal Removal. Crit Rev Environ Sci Technol 00–00. doi: 10.1080/10643389.2015.1096880

Jahirul MI, Rasul MG, Chowdhury AA, Ashwath N (2012) Biofuels production through biomass pyrolysis- A technological review. Energies 5:4952–5001. doi: 10.3390/en5124952

Keiluweit M, Kleber M (2009) Molecular-level interactions in soils and sediments: The role of aromatic π-systems. Environ Sci Technol 43:3421–3429. doi: 10.1021/es8033044

Keiluweit M, Nico PS, Johnson M, Kleber M (2010) Dynamic molecular structure of plant biomass-derived black carbon (biochar). Environ Sci Technol 44:1247–1253. doi: 10.1021/es9031419

Lehmann J (2007) Bio-energy in the black. Front Ecol Environ preprint:1. doi: 10.1890/060133

Li H, Dong X, da Silva EB, et al (2017) Mechanisms of metal sorption by biochars: Biochar characteristics and modifications. Chemosphere 178:466–478. doi: 10.1016/j.chemosphere.2017.03.072

Liu P, Liu WJ, Jiang H, et al (2012a) Modification of bio-char derived from fast pyrolysis of biomass and its application in removal of tetracycline from aqueous solution. Bioresour Technol 121:235–240. doi: 10.1016/j.biortech.2012.06.085

Liu W, Wang T, Borthwick AGL, et al (2013) Adsorption of Pb2+, Cd2+, Cu2+ and Cr3+ onto titanate nanotubes: Competition and effect of inorganic ions. Sci Total Environ 456–457:171–180. doi: 10.1016/j.scitotenv.2013.03.082

Liu Y, Zhao X, Li J, et al (2012b) Characterization of bio-char from pyrolysis of wheat straw and its evaluation on methylene blue adsorption. Desalin Water Treat 46:115–123. doi: 10.1080/19443994.2012.677408

Ma F, Peng C, Hou D, et al (2015) Citric acid facilitated thermal treatment: An innovative method for the remediation of mercury contaminated soil. J Hazard Mater 300:546–552. doi: 10.1016/j.jhazmat.2015.07.055

Ma F, Zhang Q, Xu D, et al (2014) Mercury removal from contaminated soil by thermal treatment with FeCl3 at reduced temperature. Chemosphere 117:388–393. doi: 10.1016/j.chemosphere.2014.08.012

Mohan D, Kumar H, Sarswat A, et al (2014) Cadmium and lead remediation using magnetic oak wood and oak bark fast pyrolysis bio-chars. Chem Eng J 236:513–528. doi: 10.1016/j.cej.2013.09.057

Mohan D, Pittman CU, Bricka M, et al (2007) Sorption of arsenic, cadmium, and lead by chars produced from fast pyrolysis of wood and bark during bio-oil production. J Colloid Interface Sci 310:57–73. doi: 10.1016/j.jcis.2007.01.020

Park J-H, Cho J-S, Ok YS, et al (2015) Comparison of single and competitive metal adsorption by pepper stem biochar. Arch Agron Soil Sci 340:150717092443002. doi: 10.1080/03650340.2015.1074186

Qi S, Hou D, Luo J (2017) Optimization of groundwater sampling approach under various hydrogeological conditions using a numerical simulation model. J Hydrol 552:505–515.

Rees F, Simonnot MO, Morel JL (2014) Short-term effects of biochar on soil heavy metal mobility are controlled by intra-particle diffusion and soil pH increase. Eur J Soil Sci 65:149–161. doi: 10.1111/ejss.12107

Ronsse F, van Hecke S, Dickinson D, Prins W (2013) Production and characterization of slow pyrolysis biochar: influence of feedstock type and pyrolysis conditions. GCB Bioenergy 5:104–115. doi: 10.1111/gcbb.12018

Saleh ME, El-Refaey AA, Mahmoud AH (2016) Effectiveness of sunflower seed husk biochar for removing copper ions from wastewater: a comparative study. Soil Water Res 11:53–63. doi: 10.17221/274/2014-SWR

Shen Z, Jin F, Wang F, et al (2015) Sorption of lead by Salisbury biochar produced from British broadleaf hardwood. Bioresour Technol 193:553–556. doi: 10.1016/j.biortech.2015.06.111

Shen Z, Som AM, Wang F, et al (2016) Long-term impact of biochar on the immobilisation of nickel (II) and zinc (II) and the revegetation of a contaminated site. Sci Total Environ 542:771–776.

Shen Z, Tian D, Zhang X, et al (2017a) Mechanisms of biochar assisted immobilization of Pb 2+ by bioapatite in aqueous solution. Chemosphere 190: 260-266. doi: 10.1016/j.chemosphere.2017.09.140

Shen Z, Zhang Y, Jin F, et al (2017b) Qualitative and quantitative characterisation of adsorption mechanisms of lead on four biochars. Sci Total Environ 609:1401–1410. doi: 10.1016/j.scitotenv.2017.08.008

Shen Z, Zhang Y, McMillan O, et al (2017c) Characteristics and mechanisms of nickel adsorption on biochars produced from wheat straw pellets and rice husk. Environ Sci Pollut Res 1–11. doi: 10.1007/s11356-017-8847-2

Song Y, Hou D, Zhang J, et al (2018) Environmental and socio-economic sustainability appraisal of contaminated land remediation strategies: A case study at a mega-site in China. Sci Total Environ 610–611:391–401. doi: 10.1016/j.scitotenv.2017.08.016

Tran HN, You S-J, Chao H-P (2016) Effect of pyrolysis temperatures and times on the adsorption of cadmium onto orange peel derived biochar. Waste Manag Res 34:129–138. doi: 10.1177/0734242X15615698

Uchimiya M, Cantrell KB, Hunt PG, et al (2012) Retention of Heavy Metals in a Typic Kandiudult Amended with Different Manure-based Biochars. J Environ Qual 41:1138. doi: 10.2134/jeq2011.0115

Usman A, Sallam A, Zhang M, et al (2016) Sorption Process of Date Palm Biochar for Aqueous Cd (II) Removal: Efficiency and Mechanisms. Water Air Soil Pollut. doi: 10.1007/s11270-016-3161-z

Wang Z, Han L, Sun K, et al (2016) Sorption of four hydrophobic organic contaminants by biochars derived from maize straw, wood dust and swine manure at different pyrolytic temperatures. Chemosphere 144:285–291.

doi: 10.1016/j.chemosphere.2015.08.042

Zhang H, Chen C, Gray EM, Boyd SE (2017a) Effect of feedstock and pyrolysis temperature on properties of biochar governing end use efficacy. Biomass and Bioenergy 105:136–146. doi: 10.1016/j.biombioe.2017.06.024

Zhang P, Lo I, O’Connor D, et al (2017b) High efficiency removal of methylene blue using SDS surface-modified ZnFe2O4 nanoparticles. J Colloid Interface Sci 508:39–48.